Neurobiology of Disease 43 (2011) 228–238

Contents lists available at ScienceDirect

Neurobiology of Disease

journal homepage: www.elsevier.com/locate/ynbdi

Knockdown of MLC1 in primary astrocytes causes cell vacuolation: A MLC disease cell model

Anna Duarri [a,c], Miguel Lopez de Heredia [d,i,1], Xavier Capdevila-Nortes [a,1], Margreet C. Ridder [e], Marisol Montolio [a,c], Tania López-Hernández [a], Ilja Boor [e], Chun-Fu Lien [f], Tracy Hagemann [g], Albee Messing [g], Dariusz C. Gorecki [f], Gert C. Scheper [e], Albert Martínez [h], Virginia Nunes [b,d,i], Marjo S. van der Knaap [e], Raúl Estévez [a,c,*]

[a] Sección de Fisiología, Departamento de Ciencias Fisiológicas II, Universidad de Barcelona, Spain
[b] Sección de Genética, Departamento de Ciencias Fisiológicas II, Universidad de Barcelona, Spain
[c] Centro de Investigación en Red de Enfermedades Raras (CIBERER), U-750, Spain
[d] Centro de Investigación en Red de Enfermedades Raras (CIBERER), U-730, ISCIII, Spain
[e] Department of Pediatrics/Child Neurology, VU University Medical Center, Amsterdam, the Netherlands
[f] Institute of Biomedical and Biomolecular Sciences, School of Pharmacy and Biomedical Sciences, University of Portsmouth, UK
[g] University of Wisconsin-Madison, WI, USA
[h] Department of Cell Biology, Faculty of Biology and Institute for Research in Biomedicine (IRB), Spain
[i] Laboratorio de Genética Molecular-IDIBELL, Spain

ARTICLE INFO

Article history:
Received 4 October 2010
Revised 7 March 2011
Accepted 14 March 2011
Available online 3 April 2011

Keywords:
Astrocyte
Junctions
Leukodystrophy
Volume

ABSTRACT

Megalencephalic leukoencephalopathy with subcortical cysts (MLC) is a rare type of leukodystrophy, in the majority of cases caused by mutations in the *MLC1* gene. MRI from MLC patients shows diffuse cerebral white matter signal abnormality and swelling, with evidence of increased water content. Histopathology in a MLC patient shows vacuolation of myelin, which causes the cerebral white matter swelling. MLC1 protein is expressed in astrocytic processes that are part of blood- and cerebrospinal fluid-brain barriers. We aimed to create an astrocyte cell model of MLC disease. The characterization of rat astrocyte cultures revealed MLC1 localization in cell–cell contacts, which contains other proteins described typically in tight and adherent junctions. MLC1 localization in these contacts was demonstrated to depend on the actin cytoskeleton; it was not altered when disrupting the microtubule or the GFAP networks. In human tissues, MLC1 and the protein *Zonula Occludens* 1 (ZO-1), which is linked to the actin cytoskeleton, co-localized by EM immunostaining and were specifically co-immunoprecipitated. To create an MLC cell model, knockdown of MLC1 in primary astrocytes was performed. Reduction of MLC1 expression resulted in the appearance of intracellular vacuoles. This vacuolation was reversed by the co-expression of human MLC1. Re-examination of a human brain biopsy from an MLC patient revealed that vacuoles were also consistently present in astrocytic processes. Thus, vacuolation of astrocytes is also a hallmark of MLC disease.

Introduction

Megalencephalic leukoencephalopathy with subcortical cysts (MLC) (OMIM 604004) is an unusual leukodystrophy (van der Knaap et al., 1995a, 1995b) characterized by infantile onset macrocephaly, diffuse signal abnormality, swelling of the cerebral white matter and the presence of cysts in the anterior temporal regions (van der Knaap et al., 1995a, 1995b). Diagnosis is based on clinical and MRI criteria. A brain biopsy from an MLC patient showed that myelin was vacuolated (van der Knaap et al., 1996).

The first disease chromosome locus was found in 2000 (Topcu et al., 2000) and the first disease gene in 2001 (Leegwater et al., 2001). Mutations in the *MLC1* gene are found in approximately 80% of the MLC patients (Ilja Boor et al., 2006; Leegwater et al., 2001, 2002; Montagna et al., 2006); there is evidence that other unknown genes are also involved (Blattner et al., 2003; Patrono et al., 2003). MLC1 (the protein product of *MLC1*) is an oligomeric membrane protein with some degree of homology to ion channels (Leegwater et al., 2001; Teijido et al., 2004). Mutations found in MLC patients reduce MLC1 protein expression (Duarri et al., 2008). The physiological role of MLC1 is unknown. Based on the myelin vacuolation present in MLC patients and the low homology of MLC1 to ion channels, it has been suggested that MLC1 could have a role in ion transport processes

* Corresponding author at: Universitat de Barcelona, Facultat de Medicina. Departament de Ciències Fisiològiques II, Campus de Bellvitge, Pavelló de Govern, C/Feixa llarga s/n, 08907 L'Hospitalet de Llobregat, Spain.
E-mail address: restevez@ub.edu (R. Estévez).
[1] These authors contributed equally to this study.
Available online on ScienceDirect (www.sciencedirect.com).

0969-9961/$ – see front matter © 2011 Elsevier Inc. All rights reserved.
doi:10.1016/j.nbd.2011.03.015

linked to water movements. Unfortunately, functional evidence is lacking, because no ion channel activity has been detected after expression of MLC1 in heterologous systems (Kaganovich et al., 2004; Teijido et al., 2004).

Within the brain, MLC1 is located in two populations: neurons and astrocytes (Boor et al., 2005; Schmitt et al., 2003; Teijido et al., 2004, 2007). In astrocytes, MLC1 is mainly present in the processes that are in contact with blood- and cerebrospinal fluid-brain barriers (CSF). Electron microscopic immunohistochemistry indicated that, in mouse tissue, MLC1 is located in astrocyte–astrocyte contacts and not in astrocyte–endothelial contacts (Teijido et al., 2007).

Here, we used rat primary astrocytes to understand the pathophysiological mechanisms of MLC. First, we characterized the endogenous MLC1 protein; and second, we reduced MLC1 expression and analyzed the consequences of this reduction. We then re-examined the human MLC brain tissue by EM to confirm the relevance of our findings.

Materials and methods

Animal experimentation and human samples

All the animal experimental protocols have been approved by the Animal Care and Ethics Committee of the University of Barcelona and conformed to the rules set by the Government of Catalunya.

Human brain samples have been examined, registered, classified and stored following general consensus of the European Brain Bank Network at the Institute of Neuropathology Brain Bank at the Bellvitge Hospital. The anonymized register included age and gender, minimal clinical data set, post-mortem delay and pH of the brain. Neuropathological diagnosis covered up to four neuropathological diagnoses of the primary disease and associated pathologies. Stage of the disease following internationally-accepted nomenclature is recorded in every case.

MLC brain biopsy material was obtained for diagnostic purposes, as has been described previously (van der Knaap et al., 1996).

Immunological procedures

Immune sera against N-terminal mouse MLC1 and the N4 anti-N-terminus of human MLC1 antibody were generated and characterized previously (Duarri et al., 2008; Teijido et al., 2004, 2007).

Primary culture and adenoviral transduction

Rat and mouse primary astrocyte cultures were prepared as described previously with some modifications (Duarri et al., 2008). Briefly, cortex and hippocampus were removed from newborn Sprague Dawley rats or OF1 mice (Charles River). Rat astrocyte cultures were prepared from 1 to 3 days old rats while mouse astrocyte cultures were prepared from 0 to 1 day old OF1 mice. Cerebral cortices were dissected and the meninges were carefully removed in cold sterile 0.3% BSA, 0.6% glucose in PBS. The tissue was trypsinized for 10 min at 37 °C and mechanically dissociated through a small bore fire-polished Pasteur pipette in complete DMEM medium (Dulbecco's Modified Eagle's Medium with 10% heat-inactivated fetal bovine serum (Biological Industries), 1% penicillin/streptomycin (Invitrogen) and 1% glutamine (Invitrogen) plus 40 U/ml DNase I (Sigma)). The cell suspension was pelleted and re-suspended in fresh complete DMEM, filtered through a 100-μm nylon membrane (BD Falcon) and plated into 75 cm^2 cell culture flasks (TPP). When the mixed glial cells reached confluence, contaminating microglia, oligodendrocytes and precursor cells were dislodged by mechanical agitation and removed as previously described (McCarthy and de Vellis, 1980). Astrocytes were plated in 6-well plates, at density of $4 \cdot 10^5$ cells per well, or in poly-D-lysine-coated cover slips at $7.5 \cdot 10^4$ cells in 24-well plates. Medium was changed every 3 days. In order to obtain astrocyte cultures arrested in the cell cycle, medium was replaced and cytosine β-D-arabinofuranoside (AraC, Sigma) (2 μM) was added. Similarly, Fluo-uridine/uridine or dBAMPc were added at 20/50 μg/ml or 250 μM, respectively. Cultured astrocytes were identified by their positive GFAP (Glial Fibrillary acid protein) staining (Dako), being >95% of cells GFAP positive.

Treatment of cells with colchicine (10 μg/ml, Sigma) and Taxol (10 μM, Sigma) was performed during 20 h (Sorci et al., 1998), while incubation with cytochalasin-D (10 μM, Sigma) was performed during 2 h (Nicchia et al., 2008).

Construction of adenovirus expressing HA-tagged human MLC1 and transduction of astrocytes were previously described (Duarri et al., 2008).

Immunofluorescence studies

Tissue immunohistochemistry was performed as previously described (Teijido et al., 2004, 2007).

For immunofluorescent staining of cells, these were fixed with PBS containing 3% paraformaldehyde for 15 min, blocked and permeabilized with 10% FBS and 0.1% Triton X-100 in PBS for 2 h at room temperature (RT). Primary antibodies were diluted in the same solution and incubated over-night at 4 °C. Antibodies used were already described Anti-mouse MLC1 and anti-human MLC1 (1:50), anti-ZO-1 (Zonula occludens 1) (1:100; Zymed), anti-N-Cadherin (1:100; Sigma), anti-β-Catenin (1:100; BD Transduction Lab.), anti-Occludin (1:100; Zymed), anti-Ezrin (1:200; Abcam), anti-Vinculin (1:1000; Zymed), anti-Connexin 43 (1:50; Zymed), Phalloidin-FITC (1:1000; Sigma), anti-β-Tubulin (1:1000; Chemicon), anti-GFAP (1:2000; Chemicon), anti-HA (haemagglutinin) 3 F10 (1:500; Roche), anti-β-Dystroglycan (1:100; Novacastra), anti-α-Dystroglycan (1:30; Upstate), anti-Syntrophin (1:80; Affinity Bioreagents), and anti-β-Dystrobrevin (1:200; Ambrosini's lab). Cells were washed and incubated for 2 h at RT with secondary antibodies: Alexa-488 anti-mouse, Alexa-568 anti-rabbit, Alexa-568 anti-mouse and Alexa-488 anti-rabbit (1:500 dilution; Invitrogen). Coverslips were mounted in Vectashield medium (Vector Laboratories) with 1.5 μg/ml DAPI (Sigma) and visualized using an Olympus DSU spinning disk confocal microscope. Colocalization experiments were analyzed using ImageJ (http://rsbweb.nih.gov/ij/).

Co-immunoprecipitation and Western blot

Rat brains were homogenized in immunoprecipitation buffer: 150 mM NaCl in PBS containing 1% Dodecyl-maltoside and protease inhibitors: 1 μM Pepstatin and Leupeptin, 1 mM Aprotinin and PMSF using a dounce homogenizer. Tissue lysates were incubated for 1 h at 4 °C and centrifuged (5 min at 3000×*g*) to discard large debris, and proteins were quantified by the BCA kit (Pierce). 1–2 mg of antibodies against mouse MLC1, an irrelevant IgG or BSA was covalently linked to an agarose matrix as described in manufacturer's instructions (AminoLink Plus Immobilization Kit, Pierce). Antibody-linked agarose matrix was equilibrated in immunoprecipitation buffer and tissue lysate was added in a ratio of 10 μl (corresponding to about 10 μg of antibody):100 μg of protein and incubated 2 h at 4 °C. Flowthrough was recovered by centrifugation and pellet was washed in the same buffer. Immunoprecipitates were eluted in SDS loading sample buffer for 15 min at 60 °C.

For Western blot studies, astrocyte lysates were prepared by homogenization of cells in PBS containing 1% Triton X-100 and protease inhibitors: 1 μM Pepstatin and Leupeptin, 1 mM Aprotinin and PMSF, incubated for 1 h at 4 °C and centrifugated. Supernatants were quantified using BCA kit (Pierce) and mixed with SDS loading sample buffer. Western-blot analysis was performed as described (Teijido et al., 2004). Membranes were incubated with primary antibodies: anti-MLC1 (1:100) and anti-β-Actin (1:10000, Sigma) and secondary antibodies: HRP-conjugated anti-rabbit and anti-mouse (1:10000;

Jackson), respectively. Quantification of Western blots was performed by ImageJ.

Electron microscopy

Small human cerebellum samples were obtained post-mortem (Bellvitge Hospital), fixed in 4% PFA and 0.1% glutaraldehyde in 0.12 M phosphate buffer and processed. They were cryoprotected gradually in sucrose and cryofixed by immersion in liquid propane. Freeze substitution was performed at −90 °C during 3 days in an "Automatic Freeze Substitution System" (AFS, Leica), using methanol containing 0.5% uranyl acetate as substitution medium. Infiltration was carried out in Lowicryl HM20 at −50 °C and then polymerized with UV lamps. Ultrathin sections were collected and processed for a post-embedding immunostaining. Samples were incubated with rabbit anti-N4-human MLC1 (1:10) antiserum. For double immunostaining, grids were incubated with rabbit anti-N4-human MLC1 (1:10) and mouse anti-ZO-1 (1:10). The secondary antibodies were 18 nm gold-conjugated goat anti-rabbit (British Biocell International; 1:20) and 12 nm colloidal gold-coated goat anti-mouse (British Biocell International; 1:20). In control experiments, the primary antibodies were omitted — no immunogold labeling occurred under these conditions.

MLC brain biopsy material was obtained from the right frontal region in a patient at the age of 13 years for diagnostic purposes (van der Knaap et al., 1996). Ultra-thin sections were collected on Formvar-coated copper grids, stained with lead citrate and uranyl-acetate, and examined by electron microscope (JEOL1010).

RNA interference

RNAi entry-clone (Gateway, Invitrogen) vectors were prepared using the Block-it PolII miR RNAi EmGFP expression vector kit following manufacturer's instructions. The sequence of the oligos used was: shRNA Scrambled (negative control): 5′aaatgtactgcgcgtggagacgttttggc-cactgactgacgtctccacgcagtacattt3′; shRNA756 (against rat MLC1): 5′ tgcacagcgcaaataatccatgttttggccactgactgacatggattatgcgctgtgca3′; and shRNA905 (against rat MLC1): 5′ttcaggatcaatttgcatccagttttggccactgact-gactggatgcattgatcctgaa. Entry clones were recombined using LR clonase into the vector pAdVDEST-CMV/V5. Adenoviruses were produced and titrated using flow cytometry detecting the EmGFP which is expressed together with the shRNA.

Real-time PCR

Total RNA was prepared from one 10 cm-culture plate using NucleoSpin RNA/Prot (Macherey–Nagel) as indicated by the manufacturer. RNA concentration was determined in a Nanodrop spectrophotometer. All samples had an A260/A280 ratio>1.8. RIN value was obtained with the RNA 600-nano (Agilent) following manufacturer instructions and calculated with 2100 Expert Software B.02.07 (Patch 01). All RNA samples were above 8. RNA was stored at −80 °C until further use.

800–1000 ng of total RNA were reverse-transcribed with Transcriptor First Strand cDNA synthesis kit (Roche) following manufacturer instructions at 25 °C for 10 min followed by 50 °C for 60 min, using random hexamers as primers. cDNA was stored at −80 °C. qPCR was performed with Lightcycler 480 probes master kit (Roche) following manufacturer instructions in a final volume of 10 μl, with cDNA at 1:50 dilution. The primers and UPL-probes used were designed with the ProbeFinder version 2.45 (Roche) by the on-line application (https://www.roche-applied-science.com/sis/rtpcr/upl/index.jsp?id=UP030000) considering exon spanning and trying to cover all splice variants. qPCR was run in a LightCycler 480 II on 384-well plates. Gene expression was normalized against ACTB (β-Actin) and efficiency curves were used for each of the analyzed genes. All amplifications were within the linear range. Data came from 4 different astrocyte preparations. Means of triplicates were used for each analysis. The standard deviation of the triplicates was 0.2 or lower. Data analysis was performed using LightCycler 480SW 1.5 software (Roche), MS-Access 2010 and MS-Excel 2010. Outliers and extremes were identified with SPSS v.12 and removed from the analysis. Significance was calculated using a Bootstrap method (Cleries et al., submitted). All primers used are presented in Supplementary Table 1.

Results

Expression of MLC1 in primary astrocyte cultures

Previous studies on brain tissue identified MLC1 in astrocyte–astrocyte plasma membrane contact regions in Bergmann glia and astrocytic processes surrounding blood vessels (Teijido et al., 2007). We aimed to study the role of MLC1 in astrocyte physiology to understand the molecular pathogenesis of MLC. In primary rat astrocytes, endogenous MLC1 was detected mostly in a diffuse intracellular localization through the cytoplasm. Since expression of other transporters or channels in astrocytes depends on the metabolic state of the cell (Ferroni et al., 1997), we analyzed MLC1 expression and localization in astrocyte cultures treated with compounds that block cell proliferation and/or cause cell differentiation (see Methods).

Increased protein expression was detected in arrested astrocyte long-term cultures (Fig. 1A). In these cells, MLC1 localization began to appear at the plasma membrane after 1 week (Fig. 1B), and it was clearly detected in astrocyte processes and junctions after 3 weeks in culture (Fig. 1C).

In order to clarify in which type of junctions MLC1 is located, we performed double immunofluorescence studies using different protein markers related to cell junctions or adhesion. A high degree of co-localization was observed between MLC1 and components of tight junctions such as *Zonula Occludens* 1 (ZO-1) (Fanning and Anderson, 2009) (Fig. 1D) and Occludin (Hirase et al., 1997) (Fig. 1E). Similarly, there was a high degree of co-localization with components of adherent junctions, such as β-Catenin (Perego et al., 2002) (Fig. 1F). Connexin 43 (Cx43), a typical component of astrocytic gap junctions (Rouach et al., 2000) co-localized with MLC1 partially (Fig. 1G); while MLC1 was distributed along the membrane protrusion joining two cells, Cx43 was localized in discrete spots through the membrane protrusion. Vinculin, a typical marker of focal adhesions (Kalman and Szabo, 2001) (Fig. 1H) and Ezrin, a protein located in developing astrocyte processes (Derouiche and Frotscher, 2001), did not co-localize with MLC1 (Fig. 1I). Similar co-localization patterns were found in mouse astrocytes (data not shown).

Relationship between MLC1 localization and the cytoskeleton

Next, we asked whether cytoskeleton could play a role in the localization of MLC1. For this, we used double immunostaining of MLC1 and markers of cytoskeletal elements combined with chemical and genetic inhibitors to perturb specific types of network filaments.

As shown in Fig. 2A, phalloidin-stained actin filaments were present in MLC1 positive astrocyte junctions. Partial disruption of the actin network with low concentrations of cytochalasin-D (cyt-D) caused cell shrinkage without causing disturbances in MLC1 localization (Fig. 2B). High concentrations of Cyt-D completely abolished MLC1 localization in these junctions (Fig. 2C).

In contrast, microtubules (stained with β-tubulin) were not present in MLC1-positive junctions (Fig. 2D), nor was MLC1 localization changed after microtubule disruption caused by a treatment with colchicine (Fig. 2E), or microtubule stabilization using the inhibitor taxol (Fig. 2F).

Regarding intermediate filaments, some colocalization of MLC1 and GFAP was detected within these astrocyte junctions (Fig. 2G). Transfection of cells with constructs of GFAP fused to GFP (green fluorescence protein) containing a dominant mutation (p.Arg239Cys)

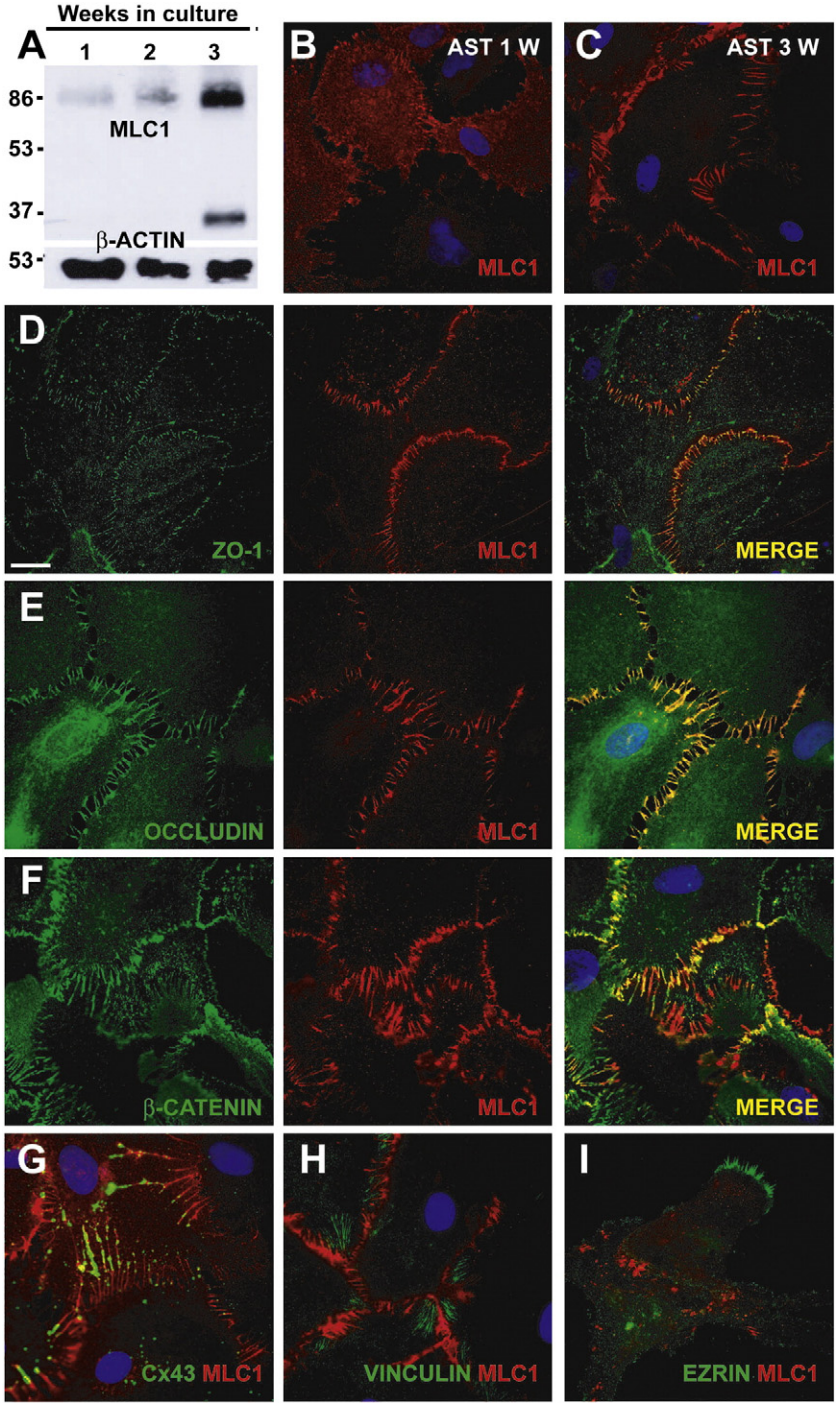

Fig. 1. Characterization of MLC1 expression in rat primary astrocyte cultures. (A) MLC1 expression analyzed by Western blot in extracts obtained from rat cortex primary astrocyte cultures arrested with AraC after 1, 2 or 3 weeks in culture. The expression of MLC1 increased with time in culture. MLC1 is detected mainly as a dimer and as a monomer. β-actin was used as a loading control. (B and C) Immunocytochemistry of MLC1 (red) in cultures of arrested astrocytes. After 1 week in culture (B), MLC1 had a diffuse cytoplasmatic labeling but also localized to contacts between astrocytes. After 3 weeks (C), MLC1 was clearly located in astrocyte–astrocyte processes. (D–F) Double labeling of MLC1 (red) with tight junction proteins ZO-1 (D) and Occludin (E), and with the adherent junction protein β-Catenin (F) (all in green), showed a large degree of co-localization (MERGE, in yellow). (G) Double immunocytochemistry experiments with Cx43, a typical gap astrocytic junction protein, showed partial co-localization with MLC1. (H–I) No co-localization was observed between MLC1 and Vinculin (H) (a typical marker of focal adhesions) and (I) Ezrin (a marker of growing astrocyte processes). Scale bar: 20 μm.

found in Alexander disease is known to disorganize astrocyte intermediate filaments formed by GFAP (Mignot et al., 2007). In astrocytes transfected with the wild-type GFAP or the GFAP R239C dominant mutant, MLC1 localization was unchanged in astrocyte junctions. Moreover, MLC1 localization was not altered in a mouse model of Alexander disease (Hagemann et al., 2006) (Supplementary Fig. 1A and B) or in a human brain from a patient with Alexander disease (de novo c.1246C>T/p.Arg416Trp mutation in GFAP) (Supplementary Fig. 1C).

Interaction of MLC1 with ZO-1

These results suggest that MLC1 localization is mainly dependent on an intact actin filament network. We reasoned that localization of MLC1

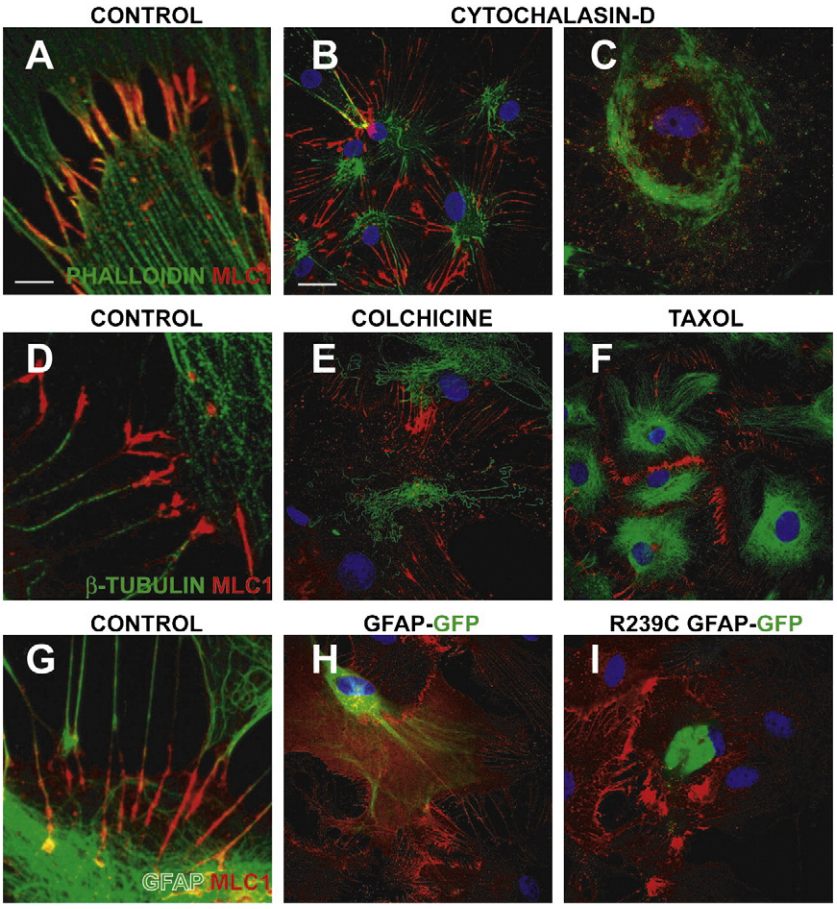

Fig. 2. Influence of the cytoskeleton on MLC1 localization in astrocytes. (A–C) *Actin cytoskeleton*. Rat primary quiescent astrocytes stained with MLC1 (red) and phalloidin (green), which stains actin filaments (A). Actin cytoskeleton depolymerization with Cytochalasin-D at 5 or 10 μM for 2 h (B and C, respectively) caused alteration of cell morphology and, at the highest drug concentration, a complete delocalization of MLC1. (D–F) *Microtubule filaments*. β-tubulin (green), did not co-localize with MLC1 (D). Colchicine (tubulin inhibitor) treatment (10 μg/ml) (E) for 20 h or (F) with 10 μM taxol (tubulin stabilizer) for 20 h triggered changes in the tubulin network, but no apparent change was observed in the localization pattern of MLC1. (G–I) *Intermediate filaments*. GFAP (green) intermediate filaments showed co-localization with MLC1 (G). Transfection of human GFAP-EmGFP fusion protein (H) or the dominant mutant R239C GFAP found in Alexander disease (I) did not cause MLC1 delocalization from cell–cell contacts. Three independent experiments gave similar results. Scale bar A, D and G: 2 μm. Scale bar for all other figures: 20 μm.

in these astrocytic junctions could also depend on interactions with the actin-binding ZO-1 protein. Therefore, co-immunoprecipitation experiments were performed (Fig. 3A). Immunoprecipitation using MLC1 antibody-coupled beads was highly efficient and specific, as almost no MLC1 was detected in the non-bound fraction and no MLC1 was detected in the immunoprecipitate with an unrelated IgG (Fig. 3A). In the MLC1 immunoprecipitate, a specific protein band around 220 kDa detected by a ZO-1 antibody was also copurified (Fig. 3A). Similar results were found using other MLC1 antibodies (data not shown).

In contrast, analogous co-immunoprecipitation experiments to detect other proteins located at astrocyte junctions (occludin, β-catenin, N-cadherin and vinculin) or those forming part of the Dystrophin Glycoprotein Complex (DGC) (Haenggi and Fritschy, 2006), which have been shown to be related with MLC1 (Ambrosini et al., 2008; Boor et al., 2007; Lanciotti et al., 2009), resulted in no co-immunoprecipitation (Supplementary Fig. 2A). Furthermore, we studied whether the ClC-2 chloride channel could be co-immunoprecipitated with MLC1, because its KO mouse displayed a myelin vacuolation similar to what has been detected in MLC patients (Blanz et al., 2007), but no co-immunoprecipitation was detected (Supplementary Fig. 2A).

To extend these results from rat astrocyte cultures to human tissues, double EM immunostainings were performed in human brain tissue. We used high-resolution EM to clearly distinguish between astrocyte–endothelial and astrocyte–astrocyte contacts around blood vessels. First, antibodies against MLC1 and β-Dystroglycan were used (Fig. 3B). The DGC protein β-Dystroglycan was used as a marker of astrocyte–endothelial junctions. As already described (Haenggi and Fritschy, 2006), small gold particles corresponding to β-Dystroglycan were detected in astrocyte membranes contacting basal laminae. In contrast, larger gold particles, corresponding to MLC1 protein, were located only at the dense junctions of point contact (puncta adhaerens) seen between astrocytes. In agreement with MLC1 not being co-localized with the DGC at points of interaction between astrocytes and endothelial cells, no change in MLC1 localization was found in several DGC-null brains including Dystrophin KO ($mdx^{\beta\text{-}geo}$), α-Dystrobrevin KO and Utrophin KO mice (Supplementary Fig. 2B–E).

Similar to rat astrocyte cultures, ZO-1 (Fig. 3C and D) colocalizes with MLC1 in astrocyte–astrocyte junctions in the human tissue. Although ZO-1 is typically expressed in endothelial cells, many groups have detected additional expression in astrocytes (Li et al., 2004; Penes et al., 2005). The specificity of the antibody used against ZO-1 was evident, since it also detected ZO-1 in endothelial cell junctions (see inset of Fig. 3C for ZO-1) (Fanning and Anderson, 2009).

Experimental approach to create an astrocyte cell model with reduced MLC1 expression

As the subcellular localization of MLC1 in quiescent primary rat astrocyte culture was found comparable to what was detected in brain

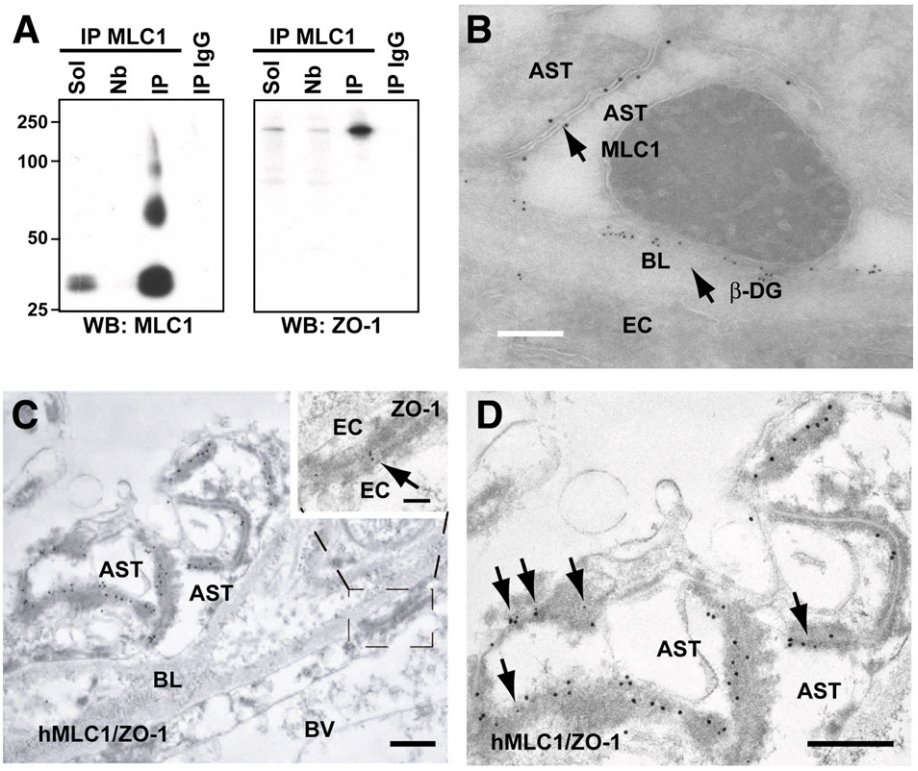

Fig. 3. Co-immunoprecipitation and colocalization of ZO-1 and MLC1 in astrocyte junctions. (A) Rat brain membranes were solubilized (Sol), and then immunoprecipitated using anti-MLC1 coupled beads. No MLC1 was detected in the not-bound (Nb) fraction or in the immunoprecipitate with an unrelated IgG (IP IgG). MLC1 immunoprecipitate showed a specific ~225 kDa protein band detected by the antibody directed against ZO-1. (B) EM double immunostaining with anti-human MLC1 and β-Dystroglycan antibodies showed that the latter is expressed in astrocyte membranes in contact with the basal lamina, whereas MLC1 is located at the cell contacts between astrocytes. Scale bar: 500 nm (C and D) Examples of double immunolabelling showing co-localization of MLC1 (18 nm gold particles) and ZO-1 (12 nm gold particles, arrows) in astrocyte–astrocyte junctions in human tissue. Anti-human MLC1 antibody showed post-embedding staining in astrocyte–astrocyte junctions and co-localized with ZO-1 (arrows in D) in human cerebellum. Note that ZO-1, but not human MLC1, is also expressed in junctions between endothelial cells (C, boxed area at higher magnification at the top right, arrows). D shows a higher magnification image observed in C. Arrows point to sites of ZO-1 expression. Scale bars in C, D: 500 nm; boxed area in C: 100 nm. BL, basal lamina; BV, Blood vessel; EC, endothelial cell; AST, astrocyte; and β-DG, β-Dystroglycan.

tissue, it was concluded that such astrocytes could be used as a cellular model to address the functions of MLC1. Recent work showed that mutations found in MLC patients cause complete lack of MLC1 protein (Duarri et al., 2008). Therefore, our next aim was to study the consequences of a reduction in the expression of MLC1 in this cell model.

We produced two adenoviral vectors each expressing a distinct shRNA (756 and 905) against rat MLC1 together with the fluorescent protein EmGFP, allowing visualization of transduced cells. A vector expressing shRNA without homology to any mammalian cDNA (SCR) was used as a control. To validate that the levels of MLC1 mRNA were reduced, we performed RT-PCR experiments 3 days after the infection with the adenovirus (performed at the multiplicity of infection (MOI) of two viruses per cell) (Fig. 4A). MLC1 mRNA levels were nearly depleted in astrocytes infected with vectors expressing shRNA directed against MLC1, but were unaffected by the control shRNA (SCR).

Time course Western blot experiments performed after transduction at the same MOI showed that 5 days after the infection, almost no MLC1 protein was detected in astrocytes infected with the MLC1 shRNA (Fig. 4B). Similar results were obtained by immunofluorescence (Fig. 4C), additionally confirming that the signal detected in astrocyte junctions in previous experiments was related to MLC1 and not to other proteins detected by our antibodies.

As an additional control, astrocytes were depleted of endogenous MLC1 by the action of shRNA, and afterwards, they were complemented with the adenovector expressing HA-tagged human MLC1 (HAhMLC1), which was resistant to this shRNA (Fig. 4C).

Next, we aimed to further deplete or totally eliminate MLC1 expression in the primary cultures. Cells infected at MOIs higher than 20 began to show signs of mortality irrespective of the adenovector, including the control type (not shown). Following further titration experiments we selected a MOI of 5 as the highest dose of vector not showing any toxic effects.

Reduction of MLC1 expression caused vacuolation of astrocytes in primary cultures and in human MLC brain

Cells depleted of MLC1 displayed intracellular vacuoles scattered through the cytosol. This effect was observed for each of the shRNAs against MLC1 (Fig. 5B and C or D for shRNA 756 and 905, respectively), but rarely occurred in non-transduced astrocytes, or astrocytes expressing the control shRNA (Fig. 5A). We quantified the number of cells showing vacuolation (defined as number of cells with at least three vacuoles of a size bigger than 0.5 μm) in seven to eight independent experiments (8 exp, N = 758 cells for shRNA SCR; 7 exp, N = 591 cells for shRNA 756; 8 exp, N = 1063 cells for shRNA 905). Vacuolation occurred in 31.9 ± 5.4% of the infected cells with shRNA 756, 32.6 ± 5.3% in cells with shRNA 905 and 6.8 ± 1.8% in the cells expressing the shRNA SCR.

To ensure that the defects observed in shRNAs directed against MLC1 transduced astrocytes were due to the lack of MLC1 and not to side effects of the shRNAs expression, co-expression experiments with human MLC1 (hMLC1) were performed (4 to 5 independent experiments; N = 654 cells for shRNA SCR + hMLC1, N = 604 cells for shRNA 756 + hMLC1, and N = 762 cells for shRNA 905 + hMLC1). As shown in Fig. 5E, cells depleted of endogenous MLC1 and complemented with human MLC1 displayed a significantly lower percentage of vacuolation (7.9 ± 1.5% versus 31.9 ± 5.4% for shRNA 756 ± hMLC1; 6.8 ± 1.7% versus 32.6 ± 5.3% for shRNA 905 ± hMLC1).

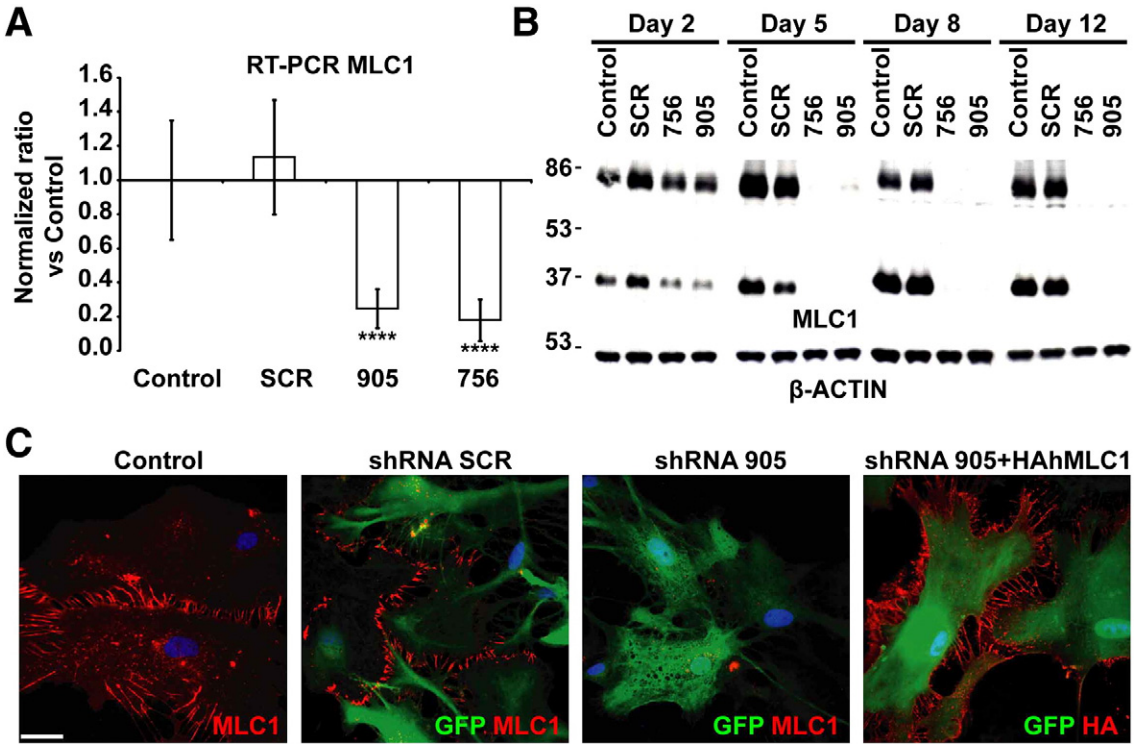

Fig. 4. Adenovector- mediated knockdown of MLC1 in rat primary astrocytes. (A) RT-qPCR experiment using specific primers to detect MLC1 mRNA. Data represent the mean ± SEM of 4 different astrocyte preparations either control or treated with indicated shRNAs. Both shRNA 756 and 905 caused almost complete inhibition of mRNA expression. ****, $P<0.0005$ (B) Astrocytes (untreated or transduced at MOI 2 with shRNA SCR, shRNA 756 and shRNA 905) were analyzed after 2, 5, 8 or 12 days by Western blot using antibodies against MLC1, which was detected mainly as a monomer and as a dimer. β-Actin was used as a loading control. Note that increasing the time after the transduction resulted in further reduction of MLC1 expression. Representative results of up to 10 different experiments are shown. (C) Control or astrocytes transduced at MOI 2, 7 days after the treatment, were fixed and processed for immunofluorescence using antibodies against MLC1. Transduced cells were visualized by the positive GFP signal. Note that MLC1 signal is detected in control cells and cells infected with the SCR shRNA but not in cells infected with the shRNA 905. Right-hand panel: cells were co-transduced with shRNA 905 at MOI 2 and HA-tagged human MLC1 (resistant to shRNA) at MOI 1. Immunofluorescence, obtained using antibodies against the HA epitope. Scale bar: 20 μm.

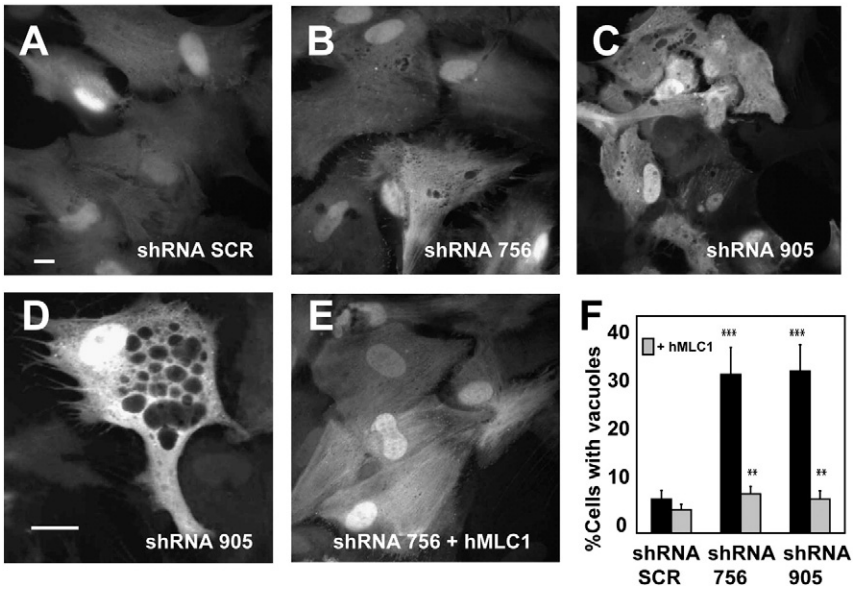

Fig. 5. Morphological alterations caused by changes in MLC1 expression. Primary culture of astrocytes were transduced with adenovectors expressing shRNA SCR (A), shRNA 756 (B) or shRNA 905 (C) at MOI 5. After 7 days cells were fixed, stained with DAPI and visualized in a CellR Imaging System. Pictures were taken using a 40× objective. Scale bar: 20 μm. (D) Typical example of an astrocyte transduced with shRNA 905 at a higher (63× objective) magnification. Vacuoles of different sizes were observed through the cytosol. Scale bar: 10 μm (E) Representative micrograph of an astrocyte transduced with adenovectors expressing shRNA 756 and human MLC1 (F) Quantification of the number of cells showing vacuolation. hMLC1: Cells transduced with the shRNA and complemented with MOI 2 of the human HA-tagged MLC1-adenovector. The data correspond to 4 to 8 independent experiments with the number of cells analyzed for each shRNA as follows: shRNA SCR (n = 758), shRNA 756 (n = 591), shRNA 905 (n = 1063), shRNA SCR + hMLC1 (n = 654), shRNA 756 + hMLC1 (n = 604), and shRNA 905 + hMLC1 (n = 762). The degree of vacuolation was quantified manually using images prepared in Adobe Photoshop. Significance was compared in the groups 756 and 905 vs SCR (black stars), and between the groups 756 and 905 versus 756 + MLC1 and 905 + MLC1, respectively (gray stars). **, $P<0.01$; ***, $P<0.005$.

Because of these results, we re-examined by electron microscopy the brain biopsy of an MLC patient (van der Knaap et al., 1996). These studies revealed again countless fluid-filled vacuoles in myelin sheaths (Fig. 6A and B), as described previously (van der Knaap et al., 1996). Additionally, vacuoles were consistently found within all perivascular astrocytic endfeet within the sections examined (Fig. 6C). Mitochondria were well preserved, indicating that the vacuole formation was not due to inadequate fixation.

The correlation between the vacuolation observed in MLC1-depleted astrocytes and the astrocytic vacuoles in MLC brain tissue suggested that this cellular model could be useful to study the pathogenesis of MLC.

Loss of MLC1 results in mRNA expression changes of transporters involved in cell volume regulation

Our first objective was to detect whether loss of MLC1 affected the levels of specific proteins associated with cell–cell junctions. Moreover, we analyzed levels of ClC-2 protein, which have also been detected in astrocyte–astrocyte junctions (Sik et al., 2000). At least three independent experiments for ZO-1, β-Catenin, Occludin, Paxillin or ClC-2 revealed no changes in expression of the respective proteins after MLC1 depletion (Fig. 7A). Similarly, no changes in protein localization were found for β-Catenin, Cx43, ZO-1 and Occludin (Supplementary Fig. 3).

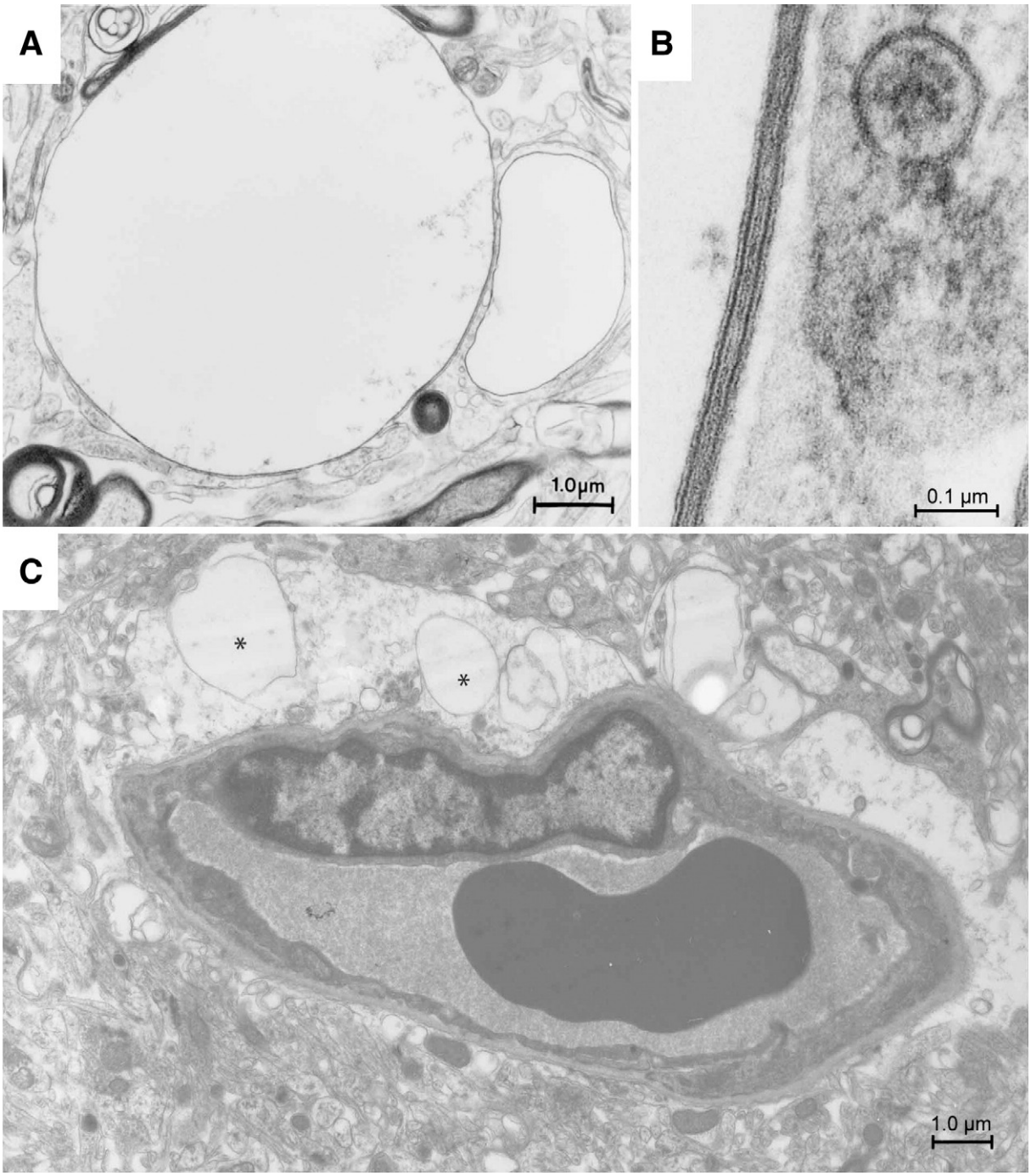

Fig. 6. Electron microscopy images of brain tissue from an MLC patient. (A) A membrane-covered vacuole is attached to a myelin sheath. (B) High magnification shows that the membrane displays the typical periodicity of myelin with the presence of major dense lines and intraperiod lines. (C) Astrocytic endfeet projecting toward a vessel also contain vacuoles (asterisks). Scale bars are shown in the lower right corner.

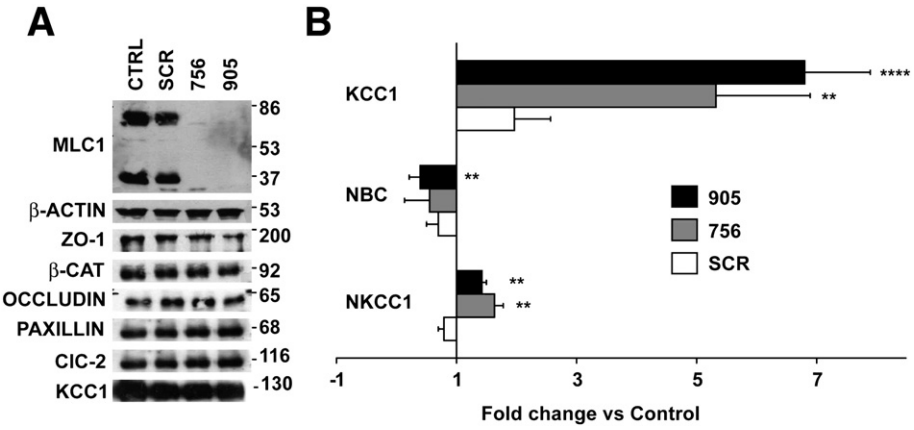

Fig. 7. Changes in expression of transporters and channels related with volume regulation. (A) 7 days after shRNA adenovector-mediated expression, cell extracts were analyzed in Western blots using antibodies against specific proteins. The result shown is representative of at least three independent experiments. Quantification using ImageJ of these different experiments revealed that levels of the different proteins studied were not statistically different in cells treated with the shRNA against MLC1 vs. controls or cells transduced with SCR shRNA (data not shown). (B) RT-qPCR experiments using specific primers to detect KCC1, NBC and NKCC1 mRNAs. Data represent the mean ± SEM of 4 different astrocyte preparations treated as indicated. **, $P<0.01$; ****, $P<0.0005$.

Unfortunately, the available antibodies against ClC-2 detected a diffuse signal in control astrocytes only, thus were not suitable for determining the localization of ClC-2 in these cells.

The homology of MLC1 to ion channels is suggestive of a function related with ion homeostasis, which would influence cell volume. Vacuolation of astrocytes with reduced MLC1 expression could also be indicative of a defect in water and/or cell volume regulation. Therefore, we measured the mRNA levels for several genes involved in cell-volume regulation in astrocytes after depletion of MLC1 (Fig. 7B). These genes included the potassium-chloride cotransporter KCC1 (Ernest et al., 2005), the sodium-bicarbonate cotransporter NBC (Nagelhus et al., 2004) and the sodium–potassium chloride cotransporter NKCC1 (Su et al., 2002), and performed real-time PCR experiments after MLC1 depletion. In four independent experiments we observed a substantial increase in expression for KCC1 (5.32 ± 1.57 fold for shRNA 756; 6.8 ± 1.1 fold for shRNA 905), a moderate increase for NKCC1 (1.63 ± 0.15 fold for shRNA 756; 1.42 ± 0.07 fold for shRNA 905) and a moderate decrease for NBC (0.55 ± 0.40 fold for shRNA 756; 0.39 ± 0.15 fold for shRNA 905). Notably, transduction with SCR shRNA also induced KCC1 expression when compared with control astrocytes (1.96 ± 0.6), but the level of induction was much higher in astrocytes infected with shRNA against MLC1. However, when analyzing at the same time point after adenoviral transduction, the levels of KCC1 protein expression by Western blot no statistical differences were observed (Fig. 7A).

Discussion

The present study extends our knowledge on the important factors for MLC1 localization in astrocytes and provides a cell model to study the pathophysiology of MLC disease.

Results obtained from rat and mouse astrocytes and from mouse and human tissue localize MLC1 in astrocyte–astrocyte contacts. Colocalization experiments between MLC1 and other junction proteins indicate that these contain components typically described in tight (Occludin, ZO-1), adherent (β-Catenin) and gap junctions (Cx43). Co-immunoprecipitation and colocalization experiments suggest that anchoring of MLC1 at these junctions involves an interaction with the adaptor molecule ZO-1. The protein ZO-1 is a member of the membrane-associated guanylate kinase (MAGUK) homologue family of proteins (Fanning and Anderson, 2009), which works as a regulated scaffold for tight junction proteins due to its ability to bind to the cortical actin cytoskeleton.

Tight junctions in astrocytes have also been described by other authors (Mack and Wolburg, 2006; Wolburg et al., 1983, 2009). A previous study (Duffy et al., 2000) reported that after treatment with Interleukin-1-beta (IL-1β), human fetal astrocytes expressed the typical tight junction molecule Claudin 1 and formed another type of junction that the authors called tight junction-like structures. An open question is whether these junctions are able to form a barrier to the flux of molecules, as several studies indicate that astrocytes do not contribute *per se* to blood-brain barrier properties in mammals (Wachtel et al., 2001). However, as astrocytic perivascular endfeet cover the vessel wall completely (Mathiisen et al., 2010), astrocytes must be involved in the exchange of water and solutes between blood and brain, although the understanding of the mechanisms employed is incomplete.

Our results indicate that MLC1 is linked to the actin cytoskeleton, as its localization was altered with cyt-D, but not when disrupting the microtubule network. MLC and Alexander disease are both leukodystrophies in which astrocytes are affected and which share some phenotypic features (Gorospe and Maletkovic, 2006). We investigated whether MLC1 localization is altered after transfection of a dominant mutant of GFAP or in Alexander disease models. This work indicates that MLC1 localization is not dramatically altered in these models, suggesting that the localization of MLC1 is not related with the integrity of the intermediate filament network. In line with this data, Vinculin, which does not colocalize with MLC1, was altered in astrocytes from GFAP mutant mice (Cho and Messing, 2009), suggesting that the integrity of the GFAP network is important for correctly located focal adhesions, but not for the stability of junctions between astrocytes.

There are differences between these and previous results from us and other groups in the localization of MLC1 (Ambrosini et al., 2008; Boor et al., 2007; Lanciotti et al., 2009). Some data suggesting that MLC1 formed part of the DGC were based on colocalization analyses using confocal microscopy (Ambrosini et al., 2008; Boor et al., 2007, 2005; Teijido et al., 2004). In view of the small distances between different membranes at and between the endfeet, a high resolution technique such as electron immunogold immunocytochemistry is advisable (Teijido et al., 2007). Taking the new data into account, we favor the idea that MLC1 is not located in areas of astrocytic processes contacting endothelial cells, but rather in areas of astrocytic processes that link astrocytes with each other. Interestingly, the DGC itself is also involved in the organization and maintenance of junctional complexes during development (Nico et al., 2003, 2004; Sjo et al., 2005). Considering the data from other authors (Ambrosini et al., 2008; Boor et al., 2007), the exact relationship between the DGC and the localization of MLC1 still needs to be clarified. An interesting unifying hypothesis that could explain these differences is that MLC1 expressed

in different compartments might associate with different protein complexes having distinct physiological roles.

Although MLC1 was coimmunoprecipitated with the ZO-1 protein, a protein detected in astrocyte cell junctions, reduction of MLC1 protein levels did not cause any alteration in protein levels or in its subcellular localization in this protein or in the other junctional proteins studied. We interpret this data as MLC1 not being necessary for the formation and maintenance of these junctions.

In agreement with the suggested role of MLC1 in ion/water homeostasis, reduction of MLC1 protein levels causes vacuolation in astrocytes. In the initial characterization of the brain biopsy of an MLC patient (van der Knaap et al., 1996), the number of large intramyelinic vacuoles was overwhelming. At re-examination of the EM tissue, we specifically focused on astrocytic processes, where MLC1 is located. This study revealed that all astrocytic processes in the sections examined consistently contain vacuoles. We conclude then that astrocytic endfeet vacuolation is also a hallmark of MLC disease. Whether the vacuoles detected in myelin are due to non-cell autonomous effects or due to the lack of MLC1 in neurons still needs to be clarified.

Similar to the vacuolation detected in MLC patients, the knockout mouse of the ClC-2 chloride channel displayed myelin vacuolation (Blanz et al., 2007). Because the knockout mice also displayed alterations in other tissues than brain, such as blindness and infertility (Bosl et al., 2001), we reasoned that *CLCN2* was unlikely to be another MLC disease gene. In agreement with this reasoning, no mutations were found in MLC patients without mutations in the *MLC1* gene and without linkage to the *MLC1* locus (Scheper et al., 2010). Our data cannot exclude that the ClC-2 protein may be involved in the pathogenesis of the disease, but indicate that there is not a direct association between MLC1 and the ClC-2 proteins.

The initial set of experiments, aimed to understand the vacuolation that occurs after MLC1 depletion, showed that these astrocytes had increased levels of mRNA for KCC1 and NKCC1. In contrast and by unknown mechanisms, the protein level of KCC1 was unchanged. These proteins have been described to play a role in Regulatory Volume Decrease (RVD) and Regulatory Volume Increase (RVI) processes in glioma cells, respectively (Ernest et al., 2005; Pasantes-Morales et al., 2006; Su et al., 2002). We speculate that the changes in the expression are a consequence of the vacuolation and do not drive this process, as vacuolation was not observed in KO mice and in patients with mutation in these genes (Delpire et al., 1999; Igarashi et al., 1999; Rust et al., 2007). The precise mechanism of how the lack of MLC1 causes the vacuolation of astrocytes still needs to be clarified.

In conclusion, this work provides the first cellular model of MLC disease, that mimics the phenotypic features found in an MLC patient. The astrocyte culture described here constitutes a good starting cell model to study the molecular basis of the processes that are involved in the pathogenesis of MLC.

Supplementary materials related to this article can be found online at doi:10.1016/j.nbd.2011.03.015.

Conflict of interest statement

The authors declare no conflict of interest.

Role of funding source

This study was supported in part by SAF 2009–07014 (RE), PS09/02672-ERARE to RE, Fundación Ramon Areces project (RE), ELA Foundation 2007-017 C4 project (RE and MSvdK), 2009 SGR 719 to RE, SAF 2009-12606-C02-02 (VN), CIBERER INTRA08/750 (RE and VN), 2009 SGR01490 to VN. RE is a recipient of an ICREA Academia prize. MCR, IB, GSC and MSvdK are supported by the Dutch Organization for Scientific Research ZonMw (TOP grant 9120.6002), the Hersenstichting (grants 10 F02(2).02, 13 F05.04 and 15 F07.30) and the Optimix Foundation for Scientific Research. D.C.G. and C-F.L. gratefully acknowledge the EU Interreg support: Advanced Microscopy Network (AdMiN) project. AM is supported by NIH grants NS-060120, NS-42803 and HD-03352.

Acknowledgments

We thank Miguel Morales, Xavier Gasull and Soledad Alcántara for initial help with primary astrocyte cultures, Logopharm GmbH for initial proteomic studies, Elena Ambrosini for the gift of antibodies against DGC proteins, Thomas J Jentsch for the gift of antibodies against ClC-2 and KCC1, Nienke Postma for performing the immunohistochemical stainings in brain tissue from a patient with Alexander disease, Gajja S. Salomons for performing mutational analysis of the GFAP gene in the patient with Alexander disease and Isidre Ferrer for providing us with human brain samples.

References

Ambrosini, E., Serafini, B., Lanciotti, A., Tosini, F., Scialpi, F., Psaila, R., Raggi, C., Di Girolamo, F., Petrucci, T.C., Aloisi, F., 2008. Biochemical characterization of MLC1 protein in astrocytes and its association with the dystrophin-glycoprotein complex. Mol. Cell. Neurosci. 37, 480–493.

Blanz, J., Schweizer, M., Auberson, M., Maier, H., Muenscher, A., Hubner, C.A., Jentsch, T.J., 2007. Leukoencephalopathy upon disruption of the chloride channel ClC-2. J. Neurosci. 27, 6581–6589.

Blattner, R., Von Moers, A., Leegwater, P.A., Hanefeld, F.A., Van Der Knaap, M.S., Kohler, W., 2003. Clinical and genetic heterogeneity in megalencephalic leukoencephalopathy with subcortical cysts (MLC). Neuropediatrics 34, 215–218.

Boor, P.K., de Groot, K., Waisfisz, Q., Kamphorst, W., Oudejans, C.B., Powers, J.M., Pronk, J.C., Scheper, G.C., van der Knaap, M.S., 2005. MLC1: a novel protein in distal astroglial processes. J. Neuropathol. Exp. Neurol. 64, 412–419.

Boor, I., Nagtegaal, M., Kamphorst, W., van der Valk, P., Pronk, J.C., van Horssen, J., Dinopoulos, A., Bove, K.E., Pascual-Castroviejo, I., Muntoni, F., et al., 2007. MLC1 is associated with the dystrophin-glycoprotein complex at astrocytic endfeet. Acta Neuropathol. 114, 403–410.

Bosl, M.R., Stein, V., Hubner, C., Zdebik, A.A., Jordt, S.E., Mukhopadhyay, A.K., Davidoff, M.S., Holstein, A.F., Jentsch, T.J., 2001. Male germ cells and photoreceptors, both dependent on close cell-cell interactions, degenerate upon ClC-2 Cl(−) channel disruption. EMBO J. 20, 1289–1299.

Cho, W., Messing, A., 2009. Properties of astrocytes cultured from GFAP over-expressing and GFAP mutant mice. Exp. Cell Res. 315, 1260–1272.

Delpire, E., Lu, J., England, R., Dull, C., Thorne, T., 1999. Deafness and imbalance associated with inactivation of the secretory Na-K-2Cl co-transporter. Nat. Genet. 22, 192–195.

Derouiche, A., Frotscher, M., 2001. Peripheral astrocyte processes: monitoring by selective immunostaining for the actin-binding ERM proteins. Glia 36, 330–341.

Duarri, A., Teijido, O., Lopez-Hernandez, T., Scheper, G.C., Barriere, H., Boor, I., Aguado, F., Zorzano, A., Palacin, M., Martinez, A., et al., 2008. Molecular pathogenesis of megalencephalic leukoencephalopathy with subcortical cysts: mutations in MLC1 cause folding defects. Hum. Mol. Genet. 17, 3728–3739.

Duffy, H.S., John, G.R., Lee, S.C., Brosnan, C.F., Spray, D.C., 2000. Reciprocal regulation of the junctional proteins claudin-1 and connexin43 by interleukin-1beta in primary human fetal astrocytes. J. Neurosci. 20, RC114.

Ernest, N.J., Weaver, A.K., Van Duyn, L.B., Sontheimer, H.W., 2005. Relative contribution of chloride channels and transporters to regulatory volume decrease in human glioma cells. Am. J. Physiol. Cell Physiol. 288, C1451–C1460.

Fanning, A.S., Anderson, J.M., 2009. Zonula occludens-1 and −2 are cytosolic scaffolds that regulate the assembly of cellular junctions. Ann. N. Y. Acad. Sci. 1165, 113–120.

Ferroni, S., Marchini, C., Nobile, M., Rapisarda, C., 1997. Characterization of an inwardly rectifying chloride conductance expressed by cultured rat cortical astrocytes. Glia 21, 217–227.

Gorospe, J.R., Maletkovic, J., 2006. Alexander disease and megalencephalic leukoencephalopathy with subcortical cysts: leukodystrophies arising from astrocyte dysfunction. Ment. Retard. Dev. Disabil. Res. Rev. 12, 113–122.

Haenggi, T., Fritschy, J.M., 2006. Role of dystrophin and utrophin for assembly and function of the dystrophin glycoprotein complex in non-muscle tissue. Cell. Mol. Life Sci. 63, 1614–1631.

Hagemann, T.L., Connor, J.X., Messing, A., 2006. Alexander disease-associated glial fibrillary acidic protein mutations in mice induce Rosenthal fiber formation and a white matter stress response. J. Neurosci. 26, 11162–11173.

Hirase, T., Staddon, J.M., Saitou, M., Ando-Akatsuka, Y., Itoh, M., Furuse, M., Fujimoto, K., Tsukita, S., Rubin, L.L., 1997. Occludin as a possible determinant of tight junction permeability in endothelial cells. J. Cell Sci. 110 (Pt 14), 1603–1613.

Igarashi, T., Inatomi, J., Sekine, T., Cha, S.H., Kanai, Y., Kunimi, M., Tsukamoto, K., Satoh, H., Shimadzu, M., Tozawa, F., et al., 1999. Mutations in SLC4A4 cause permanent isolated proximal renal tubular acidosis with ocular abnormalities. Nat. Genet. 23, 264–266.

Ilja Boor, P.K., de Groot, K., Mejaski-Bosnjak, V., Brenner, C., van der Knaap, M.S., Scheper, G.C., Pronk, J.C., 2006. Megalencephalic leukoencephalopathy with subcortical cysts: an update and extended mutation analysis of MLC1. Hum. Mutat. 27, 505–512.

Kaganovich, M., Peretz, A., Ritsner, M., Bening Abu-Shach, U., Attali, B., Navon, R., 2004. Is the WKL1 gene associated with schizophrenia? Am. J. Med. Genet. B Neuropsychiatr. Genet. 125B, 31–37.
Kalman, M., Szabo, A., 2001. Immunohistochemical investigation of actin-anchoring proteins vinculin, talin and paxillin in rat brain following lesion: a moderate reaction, confined to the astroglia of brain tracts. Exp. Brain Res. 139, 426–434.
Lanciotti, A., Brignone, M.S., Camerini, S., Serafini, B., Macchia, G., Raggi, C., Molinari, P., Crescenzi, M., Musumeci, M., Sargiacomo, M., et al., 2010. MLC1 trafficking and membrane expression in astrocytes: Role of caveolin-1 and phosphorylation. Neurobiol. Dis. 37 (3), 581–595.
Leegwater, P.A., Yuan, B.Q., van der Steen, J., Mulders, J., Konst, A.A., Boor, P.K., Mejaski-Bosnjak, V., van der Maarel, S.M., Frants, R.R., Oudejans, C.B., et al., 2001. Mutations of MLC1 (KIAA0027), encoding a putative membrane protein, cause megalencephalic leukoencephalopathy with subcortical cysts. Am. J. Hum. Genet. 68, 831–838.
Leegwater, P.A., Boor, P.K., Yuan, B.Q., van der Steen, J., Visser, A., Konst, A.A., Oudejans, C.B., Schutgens, R.B., Pronk, J.C., van der Knaap, M.S., 2002. Identification of novel mutations in MLC1 responsible for megalencephalic leukoencephalopathy with subcortical cysts. Hum. Genet. 110, 279–283.
Li, X., Ionescu, A.V., Lynn, B.D., Lu, S., Kamasawa, N., Morita, M., Davidson, K.G., Yasumura, T., Rash, J.E., Nagy, J.I., 2004. Connexin47, connexin29 and connexin32 co-expression in oligodendrocytes and Cx47 association with zonula occludens-1 (ZO-1) in mouse brain. Neuroscience 126, 611–630.
Lien, C.F., Hazai, D., Yeung, D., Tan, J., Fuchtbauer, E.M., Jancsik, V., Gorecki, D.C., 2007. Expression of alpha-dystrobrevin in blood-tissue barriers: sub-cellular localisation and molecular characterisation in normal and dystrophic mice. Cell Tissue Res. 327, 67–82.
Mack, A.F., Wolburg, H., 2006. Growing axons in fish optic nerve are accompanied by astrocytes interconnected by tight junctions. Brain Res. 1103, 25–31.
Mathiisen, T.M., Lehre, K.P., Danbolt, N.C., Ottersen, O.P., 2010. The perivascular astroglial sheath provides a complete covering of the brain microvessels: an electron microscopic 3D reconstruction. Glia 58, 1094–1103.
McCarthy, K.D., de Vellis, J., 1980. Preparation of separate astroglial and oligodendroglial cell cultures from rat cerebral tissue. J. Cell Biol. 85, 890–902.
Mignot, C., Delarasse, C., Escaich, S., Della Gaspera, B., Noe, E., Colucci-Guyon, E., Babinet, C., Pekny, M., Vicart, P., Boespflug-Tanguy, O., et al., 2007. Dynamics of mutated GFAP aggregates revealed by real-time imaging of an astrocyte model of Alexander disease. Exp. Cell Res. 313, 2766–2779.
Montagna, G., Teijido, O., Eymard-Pierre, E., Muraki, K., Cohen, B., Loizzo, A., Grosso, P., Tedeschi, G., Palacin, M., Boespflug-Tanguy, O., et al., 2006. Vacuolating megalencephalic leukoencephalopathy with subcortical cysts: functional studies of novel variants in MLC1. Hum. Mutat. 27, 292.
Nagelhus, E.A., Mathiisen, T.M., Ottersen, O.P., 2004. Aquaporin-4 in the central nervous system: cellular and subcellular distribution and coexpression with KIR4.1. Neuroscience 129, 905–913.
Nicchia, G.P., Rossi, A., Mola, M.G., Procino, G., Frigeri, A., Svelto, M., 2008. Actin cytoskeleton remodeling governs aquaporin-4 localization in astrocytes. Glia 56, 1755–1766.
Nico, B., Frigeri, A., Nicchia, G.P., Corsi, P., Ribatti, D., Quondamatteo, F., Herken, R., Girolamo, F., Marzullo, A., Svelto, M., Roncali, L., 2003. Severe alterations of endothelial and glial cells in the blood-brain barrier of dystrophic mdx mice. Glia 42, 235–251.
Nico, B., Paola Nicchia, G., Frigeri, A., Corsi, P., Mangieri, D., Ribatti, D., Svelto, M., Roncali, L., 2004. Altered blood-brain barrier development in dystrophic MDX mice. Neuroscience 125, 921–935.
Pasantes-Morales, H., Lezama, R.A., Ramos-Mandujano, G., Tuz, K.L., 2006. Mechanisms of cell volume regulation in hypo-osmolality. Am. J. Med. 119, S4–S11.
Patrono, C., Di Giacinto, G., Eymard-Pierre, E., Santorelli, F.M., Rodriguez, D., De Stefano, N., Federico, A., Gatti, R., Benigno, V., Megarbane, A., et al., 2003. Genetic heterogeneity of megalencephalic leukoencephalopathy and subcortical cysts. Neurology 61, 534–537.
Penes, M.C., Li, X., Nagy, J.I., 2005. Expression of zonula occludens-1 (ZO-1) and the transcription factor ZO-1-associated nucleic acid-binding protein (ZONAB)-MsY3 in glial cells and colocalization at oligodendrocyte and astrocyte gap junctions in mouse brain. Eur. J. Neurosci. 22, 404–418.
Perego, C., Vanoni, C., Massari, S., Raimondi, A., Pola, S., Cattaneo, M.G., Francolini, M., Vicentini, L.M., Pietrini, G., 2002. Invasive behaviour of glioblastoma cell lines is associated with altered organisation of the cadherin-catenin adhesion system. J. Cell Sci. 115, 3331–3340.
Rouach, N., Glowinski, J., Giaume, C., 2000. Activity-dependent neuronal control of gap-junctional communication in astrocytes. J. Cell Biol. 149, 1513–1526.
Rust, M.B., Alper, S.L., Rudhard, Y., Shmukler, B.E., Vicente, R., Brugnara, C., Trudel, M., Jentsch, T.J., Hubner, C.A., 2007. Disruption of erythroid K-Cl cotransporters alters erythrocyte volume and partially rescues erythrocyte dehydration in SAD mice. J. Clin. Invest. 117, 1708–1717.
Scheper, G.C., van Berkel, C.G., Leisle, L., de Groot, K.E., Errami, A., Jentsch, T.J., Van der Knaap, M.S., 2010. Analysis of CLCN2 as candidate gene for megalencephalic leukoencephalopathy with subcortical cysts. Genet. Test. Mol. Biomark. 14, 255–257.
Schmitt, A., Gofferje, V., Weber, M., Meyer, J., Mossner, R., Lesch, K.P., 2003. The brain-specific protein MLC1 implicated in megalencephalic leukoencephalopathy with subcortical cysts is expressed in glial cells in the murine brain. Glia 44, 283–295.
Sik, A., Smith, R.L., Freund, T.F., 2000. Distribution of chloride channel-2-immunoreactive neuronal and astrocytic processes in the hippocampus. Neuroscience 101, 51–65.
Sjo, A., Magnusson, K.E., Peterson, K.H., 2005. Association of alpha-dystrobrevin with reorganizing tight junctions. J. Membr. Biol. 203, 21–30.
Sorci, G., Agneletti, A.L., Bianchi, R., Donato, R., 1998. Association of S100B with intermediate filaments and microtubules in glial cells. Biochim. Biophys. Acta 1448, 277–289.
Su, G., Kintner, D.B., Sun, D., 2002. Contribution of Na(+)-K(+)-Cl(−) cotransporter to high-[K(+)](o)- induced swelling and EAA release in astrocytes. Am. J. Physiol. Cell Physiol. 282, C1136–C1146.
Teijido, O., Martinez, A., Pusch, M., Zorzano, A., Soriano, E., Del Rio, J.A., Palacin, M., Estevez, R., 2004. Localization and functional analyses of the MLC1 protein involved in megalencephalic leukoencephalopathy with subcortical cysts. Hum. Mol. Genet. 13, 2581–2594.
Teijido, O., Casaroli-Marano, R., Kharkovets, T., Aguado, F., Zorzano, A., Palacin, M., Soriano, E., Martinez, A., Estevez, R., 2007. Expression patterns of MLC1 protein in the central and peripheral nervous systems. Neurobiol. Dis. 26, 532–545.
Topcu, M., Gartioux, C., Ribierre, F., Yalcinkaya, C., Tokus, E., Oztekin, N., Beckmann, J.S., Ozguc, M., Seboun, E., 2000. Vacuoliting megalencephalic leukoencephalopathy with subcortical cysts, mapped to chromosome 22qtel. Am. J. Hum. Genet. 66, 733–739.
van der Knaap, M.S., Barth, P.G., Stroink, H., van Nieuwenhuizen, O., Arts, W.F., Hoogenraad, F., Valk, J., 1995a. Leukoencephalopathy with swelling and a discrepantly mild clinical course in eight children. Ann. Neurol. 37, 324–334.
van der Knaap, M.S., Valk, J., Barth, P.G., Smit, L.M., van Engelen, B.G., Tortori Donati, P., 1995b. Leukoencephalopathy with swelling in children and adolescents: MRI patterns and differential diagnosis. Neuroradiology 37, 679–686.
van der Knaap, M.S., Barth, P.G., Vrensen, G.F., Valk, J., 1996. Histopathology of an infantile-onset spongiform leukoencephalopathy with a discrepantly mild clinical course. Acta Neuropathol. 92, 206–212.
Wachtel, M., Bolliger, M.F., Ishihara, H., Frei, K., Bluethmann, H., Gloor, S.M., 2001. Down-regulation of occludin expression in astrocytes by tumour necrosis factor (TNF) is mediated via TNF type-1 receptor and nuclear factor-kappaB activation. J. Neurochem. 78, 155–162.
Wolburg, H., Kastner, R., Kurz-Isler, G., 1983. Lack of orthogonal particle assemblies and presence of tight junctions in astrocytes of the goldfish (Carassius auratus). A freeze-fracture study. Cell Tissue Res. 234, 389–402.
Wolburg, H., Noell, S., Mack, A., Wolburg-Buchholz, K., Fallier-Becker, P., 2009. Brain endothelial cells and the glio-vascular complex. Cell Tissue Res. 335, 75–96.